Journal of Electronics and Electrical Engineering
http://www.sciencepg.com/journal/jeee

UNIVERSAL WISER PUBLISHER

Research Article

An Analytical Model for Fields Radiated from a Resonant Circular Loop Antenna over a Homogeneous Earth

Osman M. Alsemaid [1], Sameir M. Ali Hamed [2*]

[1] Department of Electrical Engineering, Faculty of Engineering, Merowe University of Technology, Merowe, Sudan
[2] Department of Electronic Engineering, Applied College, University of Hail, Hail, Kingdom of Saudi Arabia
E-mail: sa.hamed@uoh.edu.sa

Received: 29 March 2025; **Revised:** 31 May 2025; **Accepted:** 26 June 2025

Abstract: This paper presents an analytical model for electromagnetic fields radiated from a circular loop (CL) antenna with an arbitrary current and dimensions placed horizontally over a homogeneous lossy half-space. The analysis is based on the application of the image theory and the reflection coefficient (RC) approximation approach. This method makes it much easier to evaluate the field components radiated from the antenna with quite adequate precision than the Sommerfeld integral technique, which involves the evaluation of improper integrals by numerical methods. The generic field formulas presented in the study are used to derive the axial fields, far fields, and the fields of a uniform current CL antenna over a lossy half-space as special cases. The results obtained with the proposed model for dry earth, moist earth and sea water are in good agreement with the corresponding results from FEKO simulation software, provided that the loop is operating at or near its resonant frequency and that its height above the lossy half space is greater than a tenth of the resonant wavelength.

Keywords: far fields, circular loop, lossy earth, near fields

1. Introduction

The CL antenna is a transmitting and receiving antenna that has been employed in a variety of lossless and dissipative media, including biological tissue, earth materials, and geophysical probing systems. Numerous studies have thoroughly examined and documented the radiation properties of thin-wire CL antennas over the past few decades [1–4]. Research on the CL antenna includes examining loops in free space [5–10], loops over perfect electric conducting (PEC) planes [11–15], loops close to bodies of revolution [16–20], and loops over a lossy homogeneous or layered half-space [21–34], among other scenarios. On the other hand, the radiation characteristics of CL and elliptical loop antennas at frequencies up to optical regimes were considered in [35–37].

Chang [22] and Moorthy [23] investigated the problem of a horizontal electrically large loop located above a dissipative half-space. Their analysis depends on evaluating some integrals using numerical methods. Abo-Sieda [24] considered the problem of the radiation pattern of a CL source of alternating current located in the lower half-space of two conductive media using the Hankel transform to modified Helmholtz wave equations. Parise introduced analytical expressions for a circular current loop in presence of a layered earth structure [25], on a lossy half-space [26, 27], and on layered ground

DOI: https://doi.org/10.37256/jeee.4220256878

planes [28, 29]. The works in [26, 27] were extended in [30] to derive the complete canonical solution for the problem of a large horizontal CL antenna carrying a uniform current and lying on a conducting semi-infinite half-space. Miljak presented exact analytic solutions for the electromagnetic field due to a thin uniform CL current in free space and that lying in a half-space [31].

The analysis and results of the studies in [25–30] are either involve using the small-loop approximations or the quasi-static approximations to simplify the evaluation of Sommerfeld type integrals. Moreover, they are suitable only for CL antennas with uniform current distributions and are not applicable to the practical case of electrically large loop antennas where the current distribution cannot be regarded as a uniform.

Tiwari et al. presented the TEM response for configurations of central loop, in-loop, and offset-loop over a layered earth model for arbitrary receiver positions [32]. Muzi [33] considered the problem of the mutual impedance of two coaxial loops located on the surface of a conductive ground where Gegenbauer addition theorem was used to derive a series representation for the mutual impedance between the loops. Osman et al. derived the current distribution and the input impedance of an electrically large CL antenna over a lossy earth using the well known theory of the thin-wire CL antennas along with the RC approximation [34].

The literature does not, as far as we are aware, provide an analytical solution for the electromagnetic fields of CL antennas positioned horizontally over a lossy half-space with an arbitrary current distribution and size.

This study's goal is to offer a straightforward analytical model for calculating the electromagnetic fields radiated from a CL antenna positioned horizontally over a lossy homogeneous earth. The Sommerfeld integral methodology is frequently used to solve the antenna problems over lossy dielectrics, which may be a laborious and time-consuming process because it requires evaluating improper integrals numerically.

The proposed model, which is based on the image theory and the RC approximation, is straightforward with an adequate accuracy and suitable for a variety of earth materials, such as the dry earth, the moist earth, and sea water. For an arbitrary loop size and current distribution, the model works anywhere in free space, with the exception of the loop itself. The main contribution of this research is that it provides a simple model that can be used to investigate the electromagnetic fields behavior in the near and far field regions of a CL antenna with an arbitrary current distribution placed horizontally over a homogeneous earth, provided that the antenna is not too close to the earth and operates at or near its resonant frequency. The model only applies to earth materials such as the dry earth, the moist earth, and sea water.

The sections of this paper are organized such that the vector potential of the CL is derived in Section 2 and the corresponding general field expressions in Section 3. Simplified field expressions for the uniform current loop, axial fields, and far fields are derived in Section 4 as special cases from the general field expressions. Section 5 presents results and discussion. Conclusions are included in Section 6.

2. Theoretical development

The geometry of the problem is shown in Figure 1. The radius of the loop is b and it is assumed to be made of a thin perfectly conducting wire having a radius a such that the thickness parameter is $\Omega = 2ln(2\pi b/a) \geq 10$. The loop is excited by a delta voltage source of V_0 volts at ($\phi = 0$). An $e^{j\omega t}$ time dependence is assumed throughout this paper, where t is time and ω is the angular frequency. The loop is placed horizontally at a height d over a homogeneous earth.

The earth's surface is a lossy dielectric characterized by the electrical conductivity σ and the electrical permittivity ε. The conductivity is a measure of a material's ability to conduct an electric current while permittivity is a measure of a material's ability to oppose electric field. Formations of physical parameters describing various radio wave propagation mechanisms such as wave number, scattering cross section, reflection coefficients, penetration depth, and refraction angles depend on the values of σ and ε [38].

The complex dielectric constant is defined by $\varepsilon = \varepsilon' - j\sigma/\omega$, hence the relative dielectric constant is $\varepsilon_r = \varepsilon'_r - j\sigma/\omega\varepsilon_0$. For lossy materials, $\sigma > 0$ while for lossless materials $\sigma = 0$. σ and ε of the earth's material depend on the frequency, temperature, nature of the earth's surface, and the moisture content of the earth's surface. Table 1 lists σ and ε'_r for some earth materials and sea water at 800 MHz extracted from the graphs in [38, p. 30].

Table 1. σ and ε_r' for some earth materials and sea water at 800 MHz [38, p. 30]

Material	σ (S/m)	ε_r'
Very Dry Ground (VDG)	0.00012	3
Medium Dry Ground (MDG)	0.025	15
Wet Ground (WG)	0.12	30
Sea Water (SW)	5	81

The current $I(\phi')$ on the loop can be expanded in a complex Fourier series expansion as [3, p. 460], [4, Eq. (5-22)]

$$I(\phi') = \sum_{n=-\infty}^{+\infty} I_n e^{-jn\phi'} = I_0 + 2\sum_{n=1}^{\infty} I_n \cos n\phi' \tag{1}$$

where I_n are the current coefficients.

The electromagnetic fields $(\mathbf{E}, \mathbf{H})$ at any point (r, θ, ϕ) in the space $z > 0$ due to the loop can be obtained by superimposing the fields from the loop $(\mathbf{E}_i, \mathbf{H}_i)$ and that reflected from the surface of the lossy earth $(\mathbf{E}_r, \mathbf{H}_r)$, or

$$\mathbf{E} = \mathbf{E}_i + \mathbf{E}_r, \qquad \mathbf{H} = \mathbf{H}_i + \mathbf{H}_r \tag{2}$$

The current coefficients I_n in (1) can be obtained by enforcing the boundary conditions on the surface of the loop. The boundary condition is that the total tangential electric field on the surface of the loop is zero. The tangential electric field components on the surface of the loop are the ϕ components of the incident and reflected fields E_ϕ^i and E_ϕ^r respectively, in addition to the field due to the delta source $V_0\delta(\phi')/b$. Thus, enforcing the boundary conditions, yields

$$E_\phi^i + E_\phi^r = -\frac{V_0\delta(\phi')}{b}. \tag{3}$$

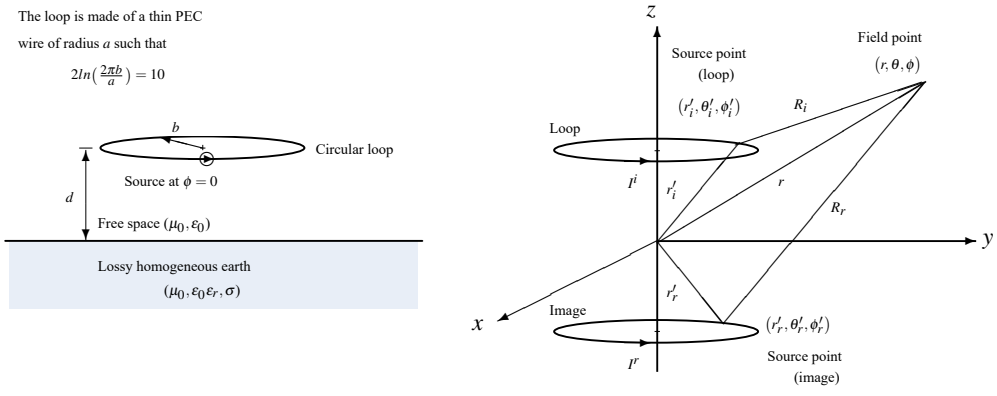

Original problem Proposed equivalent problem

Figure 1. Geometry of the problem

Using the RC approximation can help simplify the problem while maintaining a high level of accuracy. The reflected fields $(\mathbf{E}_r, \mathbf{H}_r)$ in this case are assumed to be electromagnetic fields that emanated from a coaxial image loop, as seen in Figure 1, with its center at $(0, 0, -d)$ [22]. The reflected fields have the same current as the original loop multiplied by a

factor Γ. Where Γ is the Fresnel plane-wave reflection coefficient at the interface between free space and the lossy earth. For normal incidence, Γ is given by

$$\Gamma = \begin{cases} \frac{1-\sqrt{\varepsilon_r' + \frac{\sigma}{j\omega\varepsilon_0}}}{1+\sqrt{\varepsilon_r' + \frac{\sigma}{j\omega\varepsilon_0}}}, & \text{Lossy dielectric} \\ -1, & \text{PEC plane} \end{cases}. \tag{4}$$

Based on the above assumption, the tangential fields E_ϕ^i and E_ϕ^r in (3) can be expressed as

$$E_\phi^i = \frac{j\eta_0}{4\pi}\int_0^{2\pi} I(\phi')\left[\beta b\cos(\phi-\phi') + \frac{1}{\beta b}\frac{\partial^2}{\partial\phi^2}\right]L^i d\phi' \tag{5}$$

$$E_\phi^r = \frac{j\eta_0}{4\pi}\int_0^{2\pi} \Gamma I(\phi')\left[\beta b\cos(\phi-\phi') + \frac{1}{\beta b}\frac{\partial^2}{\partial\phi^2}\right]L^r d\phi' \tag{6}$$

where

$$L^x = \frac{b}{2\pi}\int_0^{2\pi}\frac{e^{-j\beta R^x}}{R^x}d\psi \tag{7}$$

with

$$R^x(\phi-\phi') = \sqrt{4b\sin^2\left(\frac{\phi-\phi'}{2}\right) + B^x} \tag{8}$$

where $x = i$ (for the loop) or r (for the loop image), $B^i = 4a^2\sin^2\psi/2$, and $B^r = 4d^2$. η_0 and β are the characteristic impedance and the wave number of free space.

Substituting (5) and (6) into (3) and following the well-known theory of the thin-wire CL antennas [1–3], the current coefficients can be obtained as [34]

$$I_n = \frac{1}{j\pi\eta_0}\frac{V_0}{Z_n^i + \Gamma Z_n^r} \tag{9}$$

where η_0 is the characteristic impedance of free space. Z_n^i is due to the loop and Z_n^r is due to the interaction between the loop and its image. These coefficients are documented in the literature and can be expressed as

$$Z_n^x = \begin{cases} \beta b K_0^x, & n = 0 \\ \beta b\frac{K_{n-1}^x + K_{n+1}^x}{4} - \frac{n^2}{2\beta b}K_n^x, & n > 0 \end{cases} \tag{10}$$

The analytical expressions for the coefficients K_n^i and K_n^r in terms of a, b, d and β are available in [1–3] and [14] respectively.

Once the coefficients I_n are determined, then the current $I(\phi')$ in the loop is known. Consequently, the vector potential and the fields radiated from the loop can be obtained using the direct integration procedure. In a spherical system, the magnetic vector potential components of the loop and its image can be expressed as [5] and [7]

$$A_r^x = \frac{\mu_0 \beta \sin\theta}{4\pi} \int_0^{2\pi} I^x(\phi') \sin(\phi - \phi') \frac{e^{-j\beta R_x}}{R_x} d\phi' \tag{11}$$

$$A_\theta^x = \frac{\mu_0 \beta \cos\theta}{4\pi} \int_0^{2\pi} I^x(\phi') \sin(\phi - \phi') \frac{e^{-j\beta R_x}}{R_x} d\phi' \tag{12}$$

$$A_\phi^x = \frac{\mu_0 \beta}{4\pi} \int_0^{2\pi} I^x(\phi') \cos(\phi - \phi') \frac{e^{-j\beta R_x}}{R_x} d\phi' \tag{13}$$

The loop current is $I^i(\phi') = I(\phi')$ while the loop image current is $I^r(\phi') = \Gamma I(\phi')$. μ_0 is the permeability of free space and R_x is the distance between the source point $(r'_x, \theta'_x, \phi'_x)$ and the field point (r, θ, ϕ). R_x can be expressed as

$$R_x = \sqrt{r^2 + r'^2_x - 2rr'_x \cos\alpha} \tag{14}$$

where

$$\cos\alpha = \sin\theta \sin\theta'_x \cos(\phi - \phi') + \cos\theta \cos\theta'_x \tag{15}$$

Using the addition theorem, $e^{-j\beta R_x}/R_x$ can be expanded in terms of the field and source points [39, p. 292] as

$$\begin{aligned} \frac{e^{-j\beta R_x}}{R_x} = -j\beta \sum_{m=-\infty}^{+\infty} \sum_{k=m}^{+\infty} \zeta_{km} P_k^m(\cos\theta'_x) P_k^m(\cos\theta) e^{jm(\phi-\phi')} \\ \times \begin{cases} j_k(\beta r'_x) h_k^{(2)}(\beta r), & r > r'_x \\ j_k(\beta r) h_k^{(2)}(\beta r'_x), & r < r'_x \end{cases} \end{aligned} \tag{16}$$

where $j_k(\cdot)$ and $h_k^{(2)}(\cdot)$ are the spherical Bessel functions of the first and third kind of order k respectively. $P_k^m(\cdot)$ are the associate Legendre polynomials of order k and degree m. ζ_{km} is given by

$$\zeta_{km} = (2k+1) \frac{(k-m)!}{(k+m)!}. \tag{17}$$

With reference to Figure 1, it can be shown that

$$r'_r = r'_i = \sqrt{b^2 + d^2} := r_b \tag{18}$$

$$\theta_r' = \pi - \theta_i' \tag{19}$$

$$P_k^n(\cos\theta_r') = P_k^n(-\cos\theta_i') = (-1)^{k+n} P_k^n(\cos\theta_i'). \tag{20}$$

The vector potential components (A_r, A_θ, A_ϕ) at any point (r, θ, ϕ) in free space can be obtained by superimposing the vector potential components of the loop $(A_r^i, A_\theta^i, A_\phi^i)$ and that of its image $(A_r^r, A_\theta^r, A_\phi^r)$. Hence, $A_q = A_q^i + A_q^r$ where q is r, θ, or ϕ. Substituting $e^{-j\beta R_x}/R_x$ from (16) into (11)-(13) and using (1) considering that $I^i(\phi') = I(\phi')$ for the loop and $I^r(\phi') = \Gamma I(\phi')$ for its image, along with the relations (18)-(20), the vector potential components can be obtained using the same procedure followed in [7] as

$$A_r = -\frac{j\mu_0\beta\sin\theta}{2}\sum_{n=1}^{\infty}(G_{n-1} - G_{n+1})I_n \sin n\phi \tag{21}$$

$$A_\theta = -\frac{j\mu_0\beta\cos\theta}{2}\sum_{n=1}^{\infty}(G_{n-1} - G_{n+1})I_n \sin n\phi \tag{22}$$

$$A_\phi = -\frac{j\mu_0\beta}{2}\sum_{n=0}^{\infty}(G_{n-1} + G_{n+1})I_n \cos n\phi \tag{23}$$

where

$$G_m = \sum_{k=m}^{+\infty}\zeta_{km}\gamma_{km}P_k^m(\cos\theta_i')P_k^m(\cos\theta)\begin{cases} j_k(\beta r_b)h_k^{(2)}(\beta r), & r > r_b \\ j_k(\beta r)h_k^{(2)}(\beta r_b), & r < r_b \end{cases} \tag{24}$$

γ_{km} is given by

$$\gamma_{km} = 1 + (-1)^{k+m}\Gamma. \tag{25}$$

Equations (21)-(23) give the vector potential of a thin-wire CL of arbitrary radius b over a lossy earth.

3. Electromagnetic fields

Using the well known relation

$$\mathbf{H} = \frac{1}{\mu}\nabla \times \mathbf{A} \tag{26}$$

the spherical coordinates components of the magnetic field **H** can be obtained by substituting the vector potential components from (21)-(23) into (26). Thus, following [7] the magnetic field components radiated from a thin CL of radius b over a lossy earth can be written as

$$H_r = -\frac{j\beta b}{2r}\left\{ g_1^{\theta} I_0 + \sum_{n=1}^{\infty} \left[(g_{n-1}^{\theta} + g_{n+1}^{\theta}) - n\cot\theta (G_{n-1} - G_{n+1}) \right] I_n \cos n\phi \right\} \tag{27}$$

$$H_\theta = -\frac{j\beta b}{2r}\left\{ g_1^{r} I_0 + \sum_{n=1}^{\infty} \left[(g_{n-1}^{r} + g_{n+1}^{r}) - n(G_{n-1} - G_{n+1}) \right] I_n \cos n\phi \right\} \tag{28}$$

$$H_\phi = -\frac{j\beta b}{2r} \sum_{n=1}^{\infty} \left[\cos\theta (g_{n-1}^{r} - g_{n+1}^{r}) - \sin\theta (g_{n-1}^{\theta} - g_{n+1}^{\theta}) \right] I_n \sin n\phi \tag{29}$$

where

$$g_m^r = \sum_{k=m}^{+\infty} \zeta_{km} \gamma_{km} P_k^m(\cos\theta_i') P_k^m(\cos\theta) X_k \tag{30}$$

$$g_m^{\theta} = \sum_{k=m}^{+\infty} \zeta_{km} \gamma_{km} Y_{mk} \begin{cases} j_k(\beta r_b) h_k^{(2)}(\beta r), r > r_b \\ j_k(\beta r) h_k^{(2)}(\beta r_b), r < r_b \end{cases} \tag{31}$$

$$X_k = \begin{cases} j_k(\beta r_b)[\beta r h_{k-1}^{(2)}(\beta r) - k h_k^{(2)}(\beta r)], & r > r_b \\ h_k^{(2)}(\beta r_b)[\beta r j_{k-1}(\beta r) - k j_k(\beta r)], & r < r_b \end{cases} \tag{32}$$

$$Y_{mk} = [(1+m)\cot\theta P_k^m(\cos\theta) + P_k^{m+1}(\cos\theta)] P_k^m(\cos\theta_i'). \tag{33}$$

The associated electric field **E** and its components can be determined from

$$\mathbf{E} = \frac{1}{j\omega\varepsilon_0} \nabla \times \mathbf{H}. \tag{34}$$

The field expressions (27)-(29) are valid everywhere in free space except on the loop for arbitrary loop current and radius. When removing the lossy half space and letting $d = 0$, then $\Gamma \to 0$ and these expressions reduce to that obtained in [7] for an isolated loop radiating in free space.

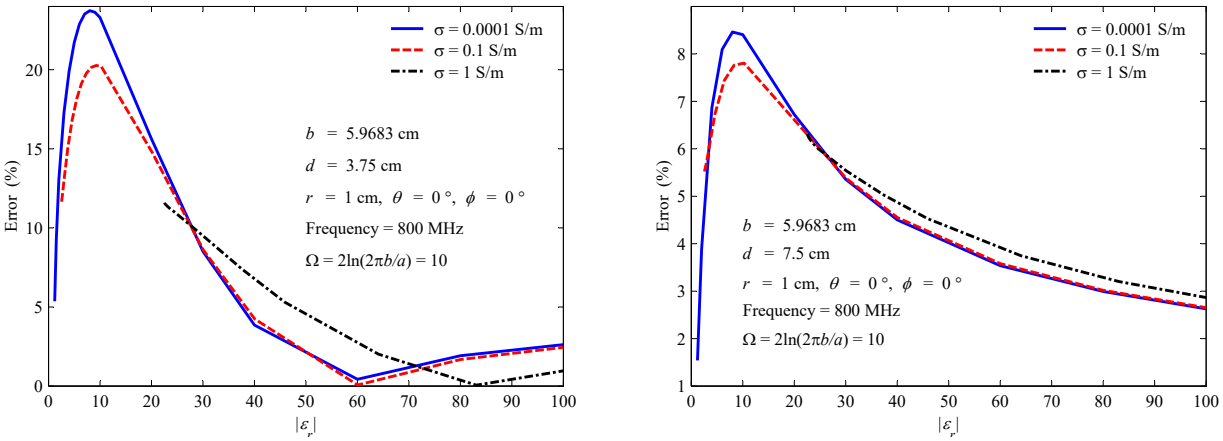

Figure 2. The percentage error between the results of this model and that obtained from FEKO [42] against $|\varepsilon_r|$ of some lossy materials for a resonant loop at heights (a) $d = 0.1\lambda$, (b) $d = 0.2\lambda$ over the material

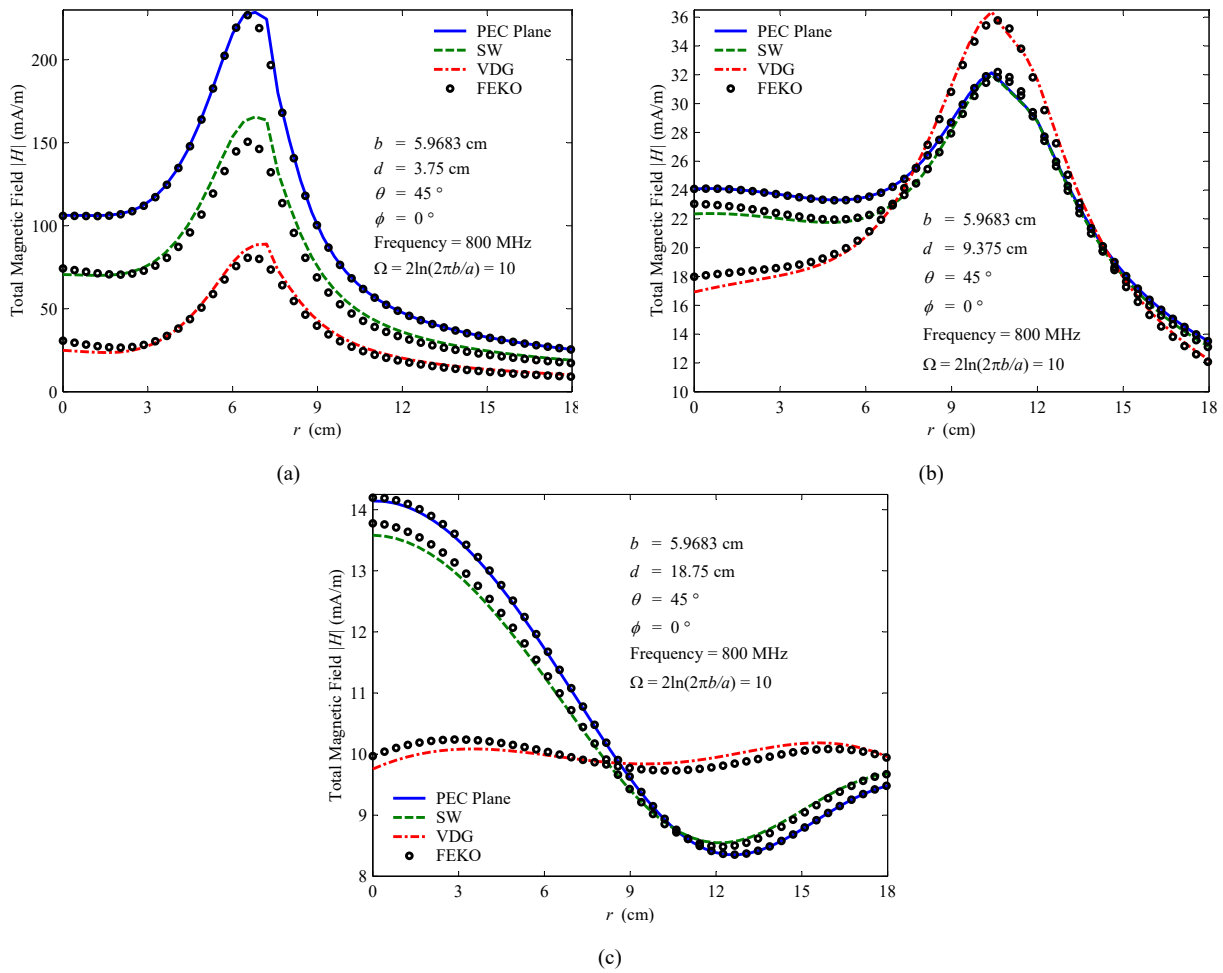

Figure 3. Total magnetic field for a resonant CL antenna at heights (a) $d = 0.1\lambda$, (b) $d = 0.25\lambda$, and (c) $d = 0.5\lambda$ over a PEC plane, SW, and a VDG

4. Special cases

4.1 *Fields of a uniform current loop*

When the current in the loop is constant, then only the term for $n = 0$ remains and all other terms vanish. Thus, $I(\phi') = I_0$ and the magnetic fields radiated from a uniform CL antenna over a lossy earth can be obtained as a special case from (27)-(29) by letting $n = 0$, which yields

$$H_r = \frac{\beta b I_0}{j2r} \sum_{k=1}^{+\infty} \zeta_{k1} \gamma_{k1} Y_{1k} \begin{cases} j_k(\beta r_b) h_k^{(2)}(\beta r), & r > r_b \\ j_k(\beta r) h_k^{(2)}(\beta r_b), & r < r_b \end{cases} \tag{35}$$

$$H_\theta = \frac{\beta b I_0}{j2r} \sum_{k=1}^{+\infty} \zeta_{k1} \gamma_{k1} P_k^1(\cos\theta_i') P_k^1(\cos\theta) X_k \tag{36}$$

and $H_\phi = 0$. The associated electric field components can be obtained by substituting H_r, H_θ, and H_ϕ into (34).

4.2 *Axial Fields*

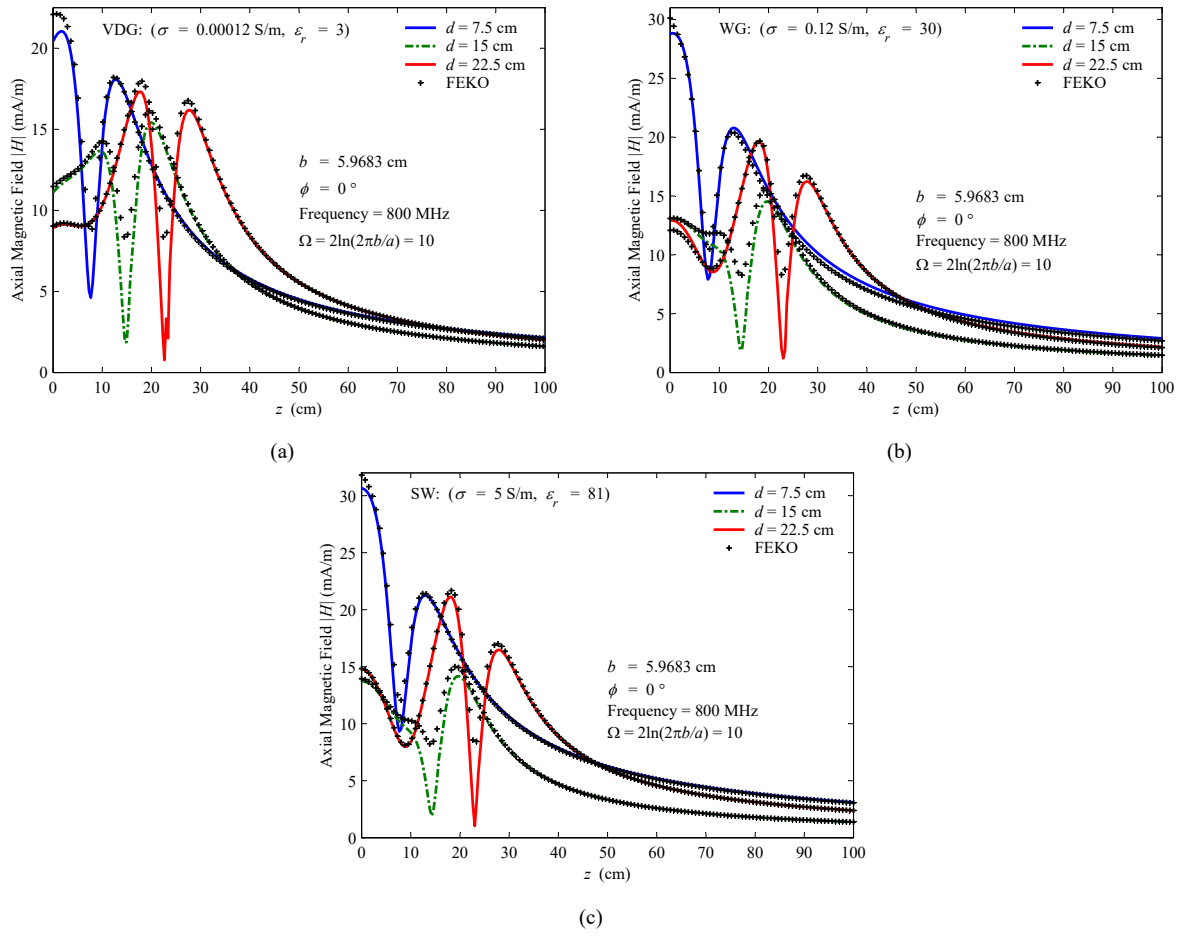

Figure 4. Axial magnetic fields for a resonant CL antenna at heights $d = 0.2\lambda$, $d = 0.4\lambda$, and $d = 0.6\lambda$ over (a) a VDG, (b) a WG, and (c) SW

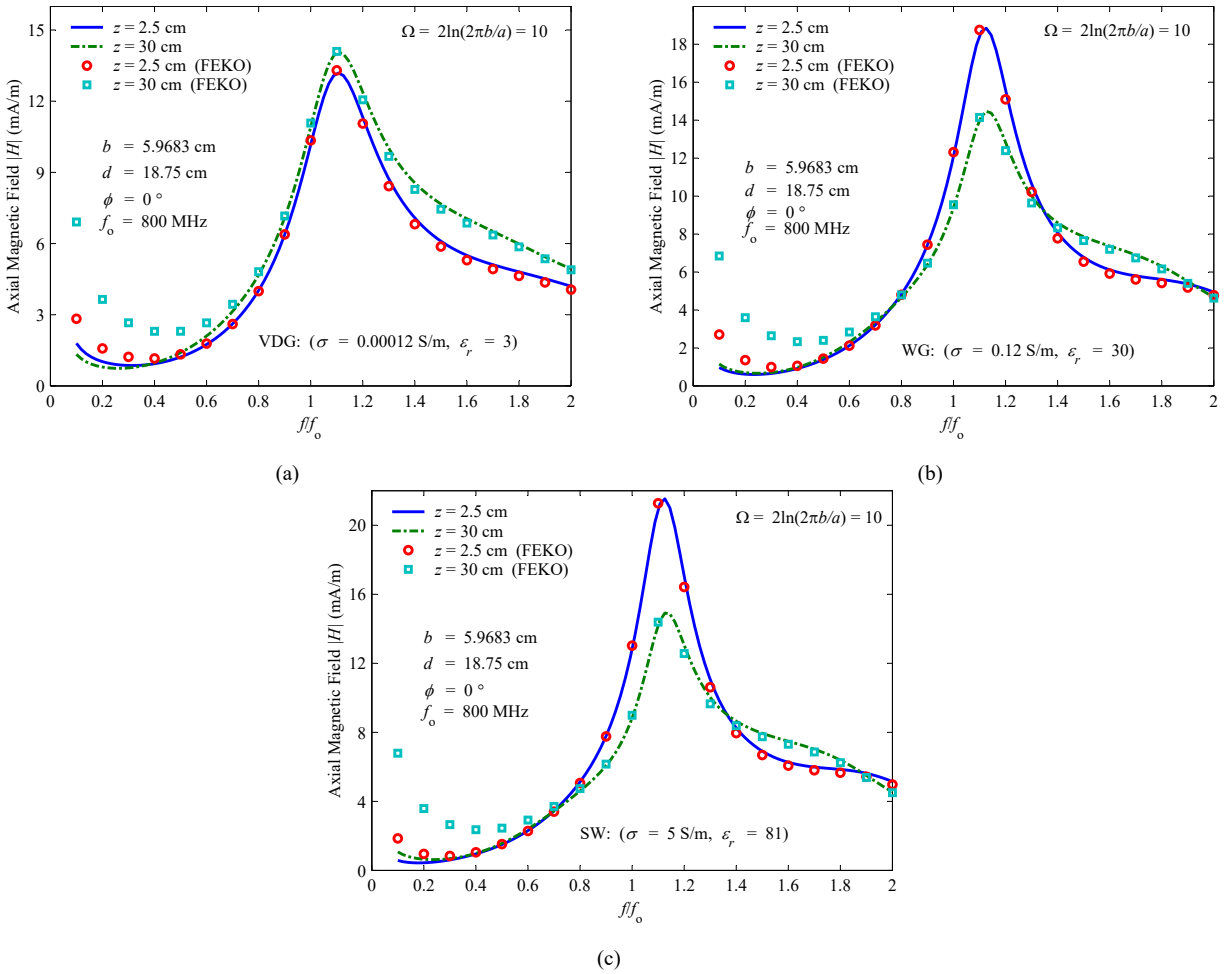

Figure 5. Axial magnetic field against frequency for a resonant CL antenna at a height $d = 0.5\lambda$ over (a) a VDG, (b) a WG, and (c) SW.

On the axis of the antenna $\theta = 0$. Using $P_k^n(1) = 1$ for $n = 0$ and $P_k^n(1) = 0$ for $n > 0$, with $\theta \to 0$,(30)-(33) can be used to show that on the axis of the loop (27)-(29) reduce to

$$H_r = -\frac{j\beta bI_0}{2r} g_1^{\theta}(\theta = 0) \tag{37}$$

$$H_\theta = -\frac{j\beta bI_1}{2r} [g_0^r(\theta = 0) - G_0(\theta = 0)] \cos\phi \tag{38}$$

$$H_\phi = -\frac{j\beta bI_1}{2r} [g_0^r(\theta = 0) - G_0(\theta = 0)] \sin\phi \tag{39}$$

4.3 *Far-Fields*

In the far-field region ($r \to \infty$) the large argument approximations for $h_k^{(2)}(\beta r)$ can be used to obtain the far-field expressions from (27)-(29). Replacing $h_k^{(2)}(\beta r)$ with its large argument approximations, which is given by [40, p. 729]

$$h_k^{(2)}(\beta r) \approx j^{k+1} \frac{e^{-j\beta r}}{\beta r} \tag{40}$$

into (24), (30), and (31) with $\frac{1}{r^2} \to 0$, it can be shown that

$$\frac{G_m}{r} \approx \frac{g_m^\theta}{r} \approx 0, \qquad g_m^r \approx e^{-j\beta r} \sum_{k=m}^{+\infty} j^k \zeta_{km} \gamma_{km} j_k(\beta r_b) P_k^m(\cos\theta_i') P_k^m(\cos\theta). \tag{41}$$

Using (41) along with [41]

$$J_n(x \sin\vartheta \sin\varphi) e^{jx\cos\vartheta\cos\varphi} = \sum_{k=0}^{\infty} j^{k-n} \frac{(k-n)!}{(k+n)!} j_k(x) P_k^n(\cos\vartheta) P_k^n(\cos\varphi) \tag{42}$$

and the Bessel function properties [40, p. 688], the approximate non-zero field expressions for a thin-wire CL of radius b over a lossy earth at the far-field region can be obtained as

$$H_\theta = -\beta b \left(1 + \Gamma e^{-j2\beta d\cos\theta}\right) e^{j\beta d\cos\theta} \frac{e^{-j\beta r}}{r} \left[\frac{J_1(u) I_0}{2} - \sum_{n=1}^{\infty} j^n J_n'(u) I_n \cos n\phi\right] \tag{43}$$

$$H_\phi = -\beta b \left(1 + \Gamma e^{-j2\beta d\cos\theta}\right) e^{j\beta d\cos\theta} \cot\theta \frac{e^{-j\beta r}}{r} \sum_{n=1}^{\infty} n j^n J_n(u) I_n \sin n\phi \tag{44}$$

where $u = \beta b \sin\theta$. $J_n(\cdot)$ is the Bessel function of the first kind of order n and $J_n'(u) = \partial J_n(u)/\partial u$. The associated electric far-field components can be determined using the well-known relations $E_\theta = \eta_0 H_\phi$ and $E_\phi = -\eta_0 H_\theta$.

5. Results and Discussion

To investigate the limits and conditions for the earth materials under which the proposed model applies, the error between the axial fields of the model and that obtained from the exact Sommerfeld integrals using FEKO [42] were computed for a resonant loop at heights $d = 0.1\lambda$ and $d = 0.2\lambda$ at $r = 1$ cm for different materials. The results are displayed in Figure 2 against the magnitude of the dielectric constant of the materials with $1.2 \leq \varepsilon_r' \leq 100$ for different cases of the conductivity ($\sigma = 0.0001$ S/m, 0.1 S/m, and 1.0 S/m).

It is clear from Figure 2(a) that the difference between the proposed model and FEKO [42] results is less than 15% for $|\varepsilon_r| \geq 20.8$ for all materials when the height of the loop is 0.1λ with their agreement improving with increasing ε_r' and σ. When the height of the loop becomes 0.2λ (Figure 2(b)) or higher, the difference does not exceed 8.45% for all materials with $\sigma \geq 0.0001$ S/m, which may include other types of lossy substrates besides earth materials.

The total magnetic field as a function of the distance r was computed from (27)-(29) for a resonant loop ($\beta b = 1$) placed horizontally above a PEC ground plane, SW, and VDG, at 800 MHz and compared to corresponding results obtained using FEKO [42]. The results were computed at heights $d = 0.1\lambda$, $d = 0.25\lambda$, and $d = 0.5\lambda$ in the plane $\theta = 45°$, $\phi = 0°$

and displayed in Figure 3. The points near $r = r_b$ are removed from the graphs, since the convergence of the solution is very slow at these points.

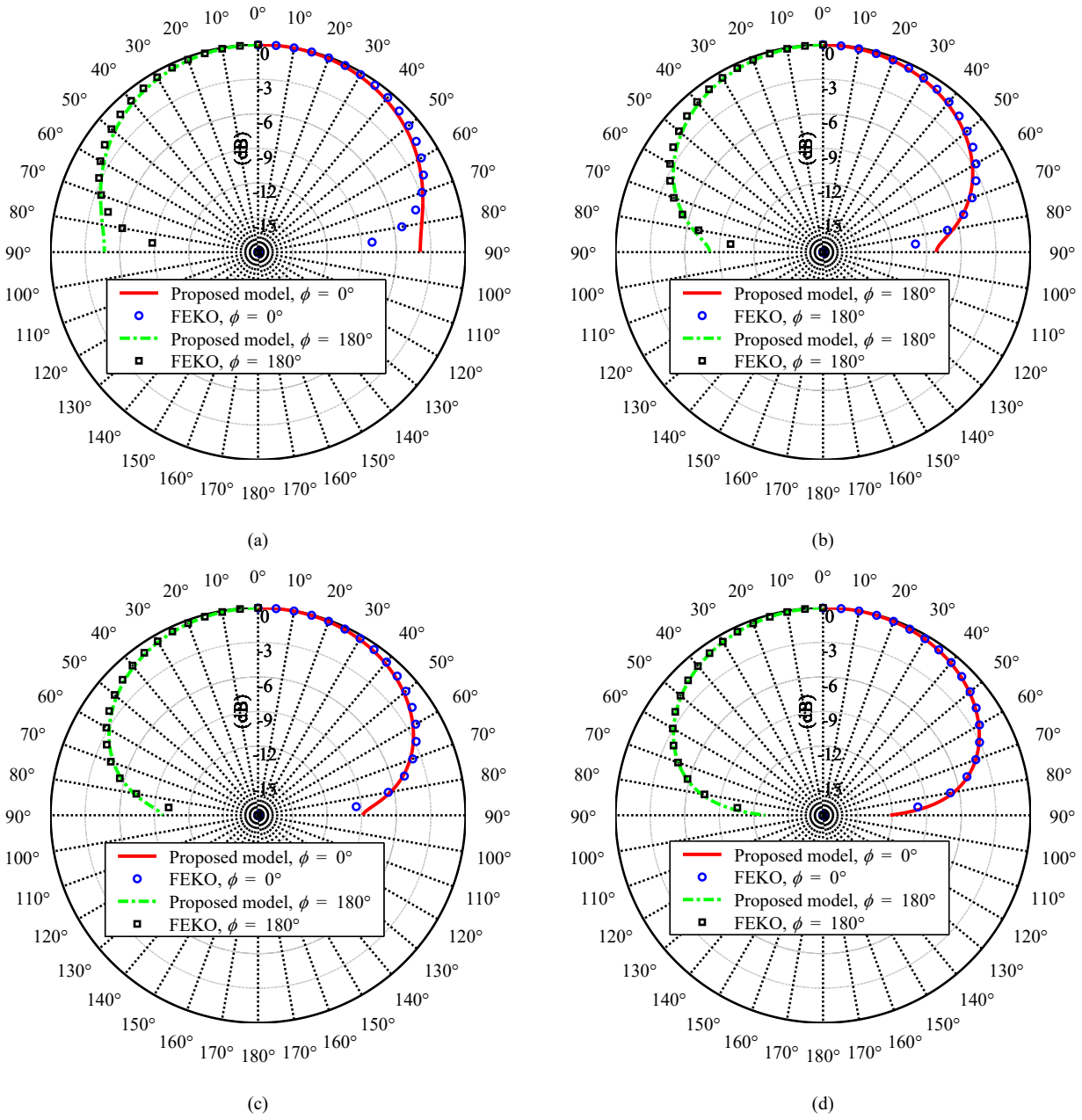

Figure 6. Normalized far field in the θ direction for a resonant CL antenna at a height $d = 0.25\lambda$ over (a) a VDG, (b) a MDG, (c) a WG, and (d) SW

It is clear from Figure 3 that the results from the model presented in this study are in a good agreement with the FEKO [42] results except in regions very close to the surface of the earth. The maximum error was relatively high when the loop was very close to the surface of the earth ($d \leq 0.1\lambda$). When the loop height was increased to $d = 0.25\lambda$ the maximum error between the results of the model and that from FEKO [42] was 6.23% and 3.09% for SW and the VDG cases, respectively. The corresponding errors for a loop at a height $d = 0.5\lambda$ were 1.43% and 2.17% respectively.

Another set of results is shown in Figure 3 and Table 2. Figure 4 displays a comparison between axial fields computed from (37)-(39) and that obtained from FEKO [42] simulation software for a resonant loop at heights 0.2λ, 0.4λ and 0.6λ above a VDG, a WG, and SW. Table 2 lists the percentage error between the axial field of this study and that obtained from FEKO [42] for the cases shown in Figure 4 in which the points around $r = r_b$ were avoided. Apart from the points around $r = r_b$ in each case, it is clear from these figures and the percentage errors shown in the table that the model presented in this study is in a good agreement with the results obtained using FEKO [42] simulation software. It is worth noting that the agreement between the two set of results becomes much better as the loop height d increases, and the model gives more accurate results for SW, since it has a higher σ and ε_r compared to the other materials.

Table 2. The percentage error of the axial magnetic field of a resonant CL antenna ($f_o = 800\,\text{MHz}$) at heights 0.2λ, 0.4λ and 0.6λ above a VDG, a WG, and SW

z (cm)	Error (%)								
	$d = 0.2\lambda$			$d = 0.4\lambda$			$d = 0.6\lambda$		
	VDG	WG	SW	VDG	WG	SW	VDG	WG	SW
0	8.07	4.73	3.85	3.82	0.16	1.46	1.46	6.43	0.20
20	1.03	4.32	0.57	4.29	5.99	4.82	10.75	3.80	7.01
40	1.39	6.15	1.11	0.69	3.10	0.75	0.57	0.23	0.57
60	1.64	6.74	1.22	0.56	2.89	0.52	0.38	1.37	0.25
80	1.65	7.04	1.28	0.38	2.63	0.42	0.37	2.13	0.11
100	1.66	7.19	1.30	0.03	2.40	0.35	0.37	2.66	0.05

To show the effect of the frequency on the behavior of the near fields radiated from a loop over homogeneous earth, the axial magnetic field was computed and plotted as shown Figure 5 in the frequency range $0.1f_o \leq f \leq 2f_o$ (where $f_o = 800\,\text{MHz}$ is the resonant frequency). The loop height was $d = 18.75\,\text{cm}$ and the field were computed at the points $z = 2.5\,\text{cm}$ and $z = 30\,\text{cm}$. The maximum error between the results obtained from the model of this study and the corresponding FEKO [42] results in the frequency range $0.65f_o \leq f \leq 2f_o$ were 3.53%, 3.55%, and 3.77% for the VDG, the WG, and SW respectively, which shows the good agreement between our model and the results from FEKO [42] around the resonant frequency of the loop.

Figure 6 shows a comparison between the far field radiation patterns computed from (43) and (44) with that obtained from FEKO [42] simulation software of a resonant CL antenna at a height $h = 0.25\lambda$ over a VDG, a MDG, a WG, and SW. These radiation patterns show that the model of this study deviates from FEKO results near the interface $z = 0$ for the case of VDG ($\sigma = 0.00012\,\text{S/m}$, $\varepsilon_r = 3$). For the MDG, the WG, and SW, the model gives good results. The field in the plane $\phi = 0^\circ$ is slightly greater than that in the plane $\phi = 180^\circ$. This is due to the presence of the excitation source in the plane $\phi = 0^\circ$.

The above results demonstrate that the model of this study is in a good agreement with the exact Sommerfeld integrals for various earth materials provided that the height of the loop above the earth is greater than 0.1λ and it operates around its resonant frequency.

6. Conclusion

Understanding the radiation properties of the loop antenna close to lossy materials is necessary for a variety of applications involving CL antennas, including biological tissue, earth materials, and geophysical probing systems. A straightforward analytical model for examining the behavior of electromagnetic fields radiated from a resonant CL antenna over a lossy earth is presented in this research. The model gives accurate results for earth with different electrical properties and sea water provided that the loop is operating at or close to its resonant frequency and its height above the earth is greater thana tenth of the resonant wavelength.

Conflicts of Interest

The authors declare no conflicts of interest.

References

[1] King RB, Smith GS. *Antenna in Matter: Fundamentals, Theory and Applications*. Cambridge, MA, USA: MIT Press; 1981.

[2] Wu TT. Theory of the thin circular loop antenna. *Journal of Mathematical Physics*. 1962; 3(6): 1306–1304.

[3] King RW. The loop antenna for transmission and reception. In: Collin R E, Zucker F J, editors. *Antenna Theory, Part I*. New York, USA: McGraw-Hill; 1969. p. 458–481.

[4] Smith GS. Loop antennas. In: Johnson R C, Jasik H, editors. *Antenna Engineering Handbook*. New York, USA: McGraw-Hill; 2007. Ch 5.

[5] Werner DH. Lommel Expansions in Electromagnetics. In: Werner D H, Mittra R, editors. *Frontiers in Electromagnetics*. New York, USA: IEEE Press; 2000. p. 474–522.

[6] Conway JT. New exact solution procedure for the near fields of the general thin circular loop antenna. *IEEE Transactions on Antennas and Propagation*. 2005; 53(1): 509–517. https://doi.org/10.1109/TAP.2004.838804.

[7] Hamed SM. Exact field expressions for circular loop antennas using spherical functions expansion. *IEEE Transactions on Antennas and Propagation*. 2013; 61(6): 2956–2963. https://doi.org/10.1109/TAP.2013.2250241.

[8] Hamed SM, Bashir SO. New fields expressions of a traveling wave circular loop antenna. In: *IEEE 2013 International Conference on Computing, Electrical and Electronic Engineering (ICCEEE)*; Khartoum, Sudan; 2013. p. 300–305. https://doi.org/10.1109/ICCEEE.2013.6633951.

[9] Salem MM, Caloz C. Electromagnetic fields radiated by a circular loop with arbitrary current. *IEEE Transactions on Antennas and Propagation*. 2015; 63(1): 442–446. https://doi.org/10.1109/TAP.2014.2368579.

[10] Fang Y, Zhang Y. Theory and analysis of the loop antenna and Ω-shaped loop-dipole antenna. *IEEE Open Journal of Antennas and Propagation*. 2022; 3: 1161–1171. https://doi.org/10.1109/OJAP.2022.3211345.

[11] Osman AM, Hamed SM. Exact field expressions for a concentric circular-loops antenna above a PEC ground plane. In: *IEEE 2015 International Conference on Computing, Control, Networking, Electronics and Embedded Systems Engineering (ICCNEEE)*; Khartoum, Sudan; 2015. p. 74–78. Available from: https://doi.org/10.1109/ICCNEEE.2015.7381432.

[12] Hamed SM, Osman AM. Design Formulas for Broadband Concentric Circular-Loops Antennas. *Advanced Electromagnetics*. 2015; 4(1): 45–51. https://doi.org/10.7716/aem.v4i1.277.

[13] Ayorinde AO, Adekola SA, Mowete AI. Analysis of a circular-loop antenna backed by a circular ground-plane of finite extent. In: *2017 Progress In Electromagnetics Research Symposium–Spring (PIERS)*; St. Petersburg, Russia; 2017. p. 173–179. Available from: https://doi.org/10.1109/PIERS.2017.8261728.

[14] Hejase HAN, Gedney SD, Whites KW. Effect of a finite ground plane on radiated emissions from a circular loop antenna. *IEEE Transactions on Electromagnetic Compatibility*. 1994; 36(4): 364–371. https://doi.org/10.1109/15.328868.

[15] Shoamanesh A, Shafai L. Characteristics of circular loop antennas above a lossless ground plane. *IEEE Transactions on Antennas and Propagation*. 1981; 29(3): 528–529. https://doi.org/10.1109/TAP.1981.1142607.

[16] Halder P, Ghosh B, Haque SK, Sarabandi K. Loop antenna over a conducting cone with a spherical cap. *IET Microwaves, Antennas & Propagation*. 2019; 13(14): 2559–2568. https://doi.org/10.1049/iet-map.2019.0273.

[17] Hamed SM, Bashir SO. Characteristics of a circular loop antenna in the presence of a coaxial conducting BOR attached to a planar reflector. *IEEE Antennas and Wireless Propagation Letters*. 2013; 12: 793–796. https://doi.org/10.1109/LAWP.2013.2270949.

[18] Hamed SM, Abbas MA. Radiation from a circular loop antenna placed coaxially relative to a conducting body of revolution. *IEEE Transactions on Antennas and Propagation*. 2012; 60(10): 4937–4940. https://doi.org/10.1109/TAP.2012.2207338.

[19] Partal HP, Mautz JR, Arvas E. The exact analytical solution for large circular loops radiating around a dielectric coated conducting sphere. *IEEE Transactions on Antennas and Propagation*. 2009; 57(2): 436–443. https://doi.org/10.1109/TAP.2008.2011179.

[20] Partal HP, Mautz JR, Arvas E. Radiation from a circular loop in the presence of spherically symmetric conducting or dielectric objects. *IEEE Transactions on Antennas and Propagation*. 2000; 48(10): 1646–1652. https://doi.org/10.1109/8.899681.

[21] Lincan Y, Miguel R. Magnetic field above stratified earth in magnetic loop through-the-earth wireless communications. *Radio Science*. 2022; 57(3). https://doi.org/10.1029/2021RS007388.

[22] Chang DC. Characteristics of a horizontal circular loop antenna over a multilayered, dissipative half-space. *IEEE Transactions on Antennas and Propagation*. 1973; 21(6): 871–874. https://doi.org/10.1109/TAP.1973.1140599.

[23] Moorthy S. Analysis of a thin circular loop antenna over a homogeneous earth. *The Bell System Technical Journal*. 1970; 49(6): 1215–1233. https://doi.org/10.1002/j.1538-7305.1970.tb01821.x.

[24] Abo-Seida OM. Electromagnetic fields of thin circular loop antenna of arbitrary radius. *Canadian Journal of Physics*. 2002; 80(1): 29–37. https://doi.org/10.1139/p01-127.

[25] Parise M. Fast computation of the forward solution in controlled-source electromagnetic sounding problems. *Progress In Electromagnetics Research*. 2011; 111: 119–139. https://doi.org/10.2528/PIER11012603.

[26] Parise M. An exact series representation for the EM field from a circular loop antenna on a lossy half-space. *IEEE Antennas and Wireless Propagation Letters*. 2014; 13: 23–26. https://doi.org/10.1109/LAWP.2013.2296149.

[27] Parise M. Quasi-static Vertical Magnetic Field of a Large Horizontal Circular Loop Located at the Earth's Surface. *Progress In Electromagnetics Research Letters*. 2016; 62: 29–34. https://doi.org/10.2528/PIERL16053003.

[28] Parise M. On the surface fields of a small circular loop antenna placed on plane stratified earth. *International Journal of Antennas and Propagation*. 2015; 2015: 187806. https://doi.org/10.1155/2015/187806.

[29] Parise M. Full-wave analytical explicit expressions for the surface fields of an electrically large horizontal circular loop antenna placed on a layered ground. *IET Microwaves, Antennas & Propagation*. 2017; 11(6): 929–934. https://doi.org/10.1049/iet-map.2016.0590.

[30] Parise M, Muzi M, Antonini G. Loop antennas with uniform current in close proximity to the earth: canonical solution to the surface-to-surface propagation problem. *Progress In Electromagnetics Research B*. 2017; 77: 57–69. https://doi.org/10.2528/PIERB17042005.

[31] Miljak DG. Exact expressions for the near field of a thin uniform circular loop current with application to loops lying on a half space. *Progress In Electromagnetics Research B*. 2024; 105: 93–105. https://doi.org/10.2528/PIERB24011205.

[32] Tiwari AK, Maurya PK, Singh NP. TEM response of a large loop source over the multilayer earth models. *International Journal of Geophysics*. 2018; 2018: 9891548. https://doi.org/10.1155/2018/9891548.

[33] Muzi M. An exact expression for the mutual impedance between coaxial circular loops on a homogeneous ground. *Progress In Electromagnetics Research Letters*. 2019; 81: 65–70. https://doi.org/10.2528/PIERL18110902.

[34] Osman MA, Sameir MH, Saif AM. A series solution for the input admittance of a circular loop antenna over a lossy earth. *Recent Advances in Electrical & Electronic Engineering*. 2019; 12(2): 113–117. https://doi.org/10.2174/2352096511666180523094647.

[35] McKinley AF. Theory of Impedance Loaded Loop Antennas and Nanorings From RF to Optical Wavelengths. *IEEE Transactions on Antennas and Propagation*. 2017; 65(5): 2276–2281. https://doi.org/10.1109/TAP.2017.2682219.

[36] Nagar J, McKinley AF, Werner DH. Far-field radiation properties of impedance-loaded loop antennas from RF to optical frequencies. In: *12th European Conference on Antennas and Propagation (EuCAP 2018)*; London, UK; 2018. p. 1–5. Available from: https://doi.org/10.1049/cp.2018.1114.

[37] Pantoja MF, Chaky RJ, McKinley AF, Werner DH. Essential Characteristics of Thin-Wire Elliptical Loops. *IEEE Transactions on Antennas and Propagation*. 2024; 72(2): 1107–1117. https://doi.org/10.1109/TAP.2023.3339965.

[38] *Electrical characteristics of the surface of the Earth*. Recommendation ITU-R P.527-6; 2021.

[39] Harrington RF. *Time-Harmonic Electromagnetic Fields*. New York, NY, USA: IEEE Press; 2001.

[40] George BA, Hans JW. *Mathematical Methods for Physicists*. Burlington, MA, USA: Elsevier Academic Press; 2001.

[41] Cregg PJ, Svedlindh P. Comment on: Analytical results for Bessel function times Legendre polynomials class integrals. *Journal of Physics A: Mathematical and Theoretical*. 2007; 40(47): 14029–14031. https://doi.org/10.1088/1751-8113/40/47/N01.

[42] *FEKO Electromagnetic Analysis Software release 2023.1*. Altair Engineering Inc.; 2023. Available from: https://altair.com/feko.